Eur Radiol (2014) 24:223–231
DOI 10.1007/s00330-013-3002-z

HEAD AND NECK

Head and neck tumours: combined MRI assessment based on IVIM and TIC analyses for the differentiation of tumors of different histological types

Misa Sumi · Takashi Nakamura

Received: 4 July 2013 / Revised: 9 August 2013 / Accepted: 11 August 2013 / Published online: 8 September 2013
© European Society of Radiology 2013

Abstract
Objectives We evaluated the combined use of intravoxel incoherent motion (IVIM) and time-signal intensity curve (TIC) analyses to diagnose head and neck tumours.
Methods We compared perfusion-related parameters (*PP*) and molecular diffusion values (*D*) determined from IVIM theory and TIC profiles among 92 tumours with different histologies.
Results IVIM parameters (*f* and *D* values) and TIC profiles in combination were distinct among the different types of head and neck tumours, including squamous cell carcinomas (SCCs), lymphomas, malignant salivary gland tumours, Warthin's tumours, pleomorphic adenomas and schwannomas. A multiparametric approach using both IVIM parameters and TIC profiles differentiated between benign and malignant tumours with 97 % accuracy and diagnosed different tumour types with 89 % accuracy.
Conclusions Combined use of IVIM parameters and TIC profiles has high efficacy in diagnosing head and neck tumours.
Key points
- *Head and neck tumours have wide MR perfusion/diffusion properties.*
- *Dynamic contrast-enhanced (DCE) MR imaging can characterise tumour perfusion (TIC analysis).*
- *Intravoxel incoherent motion (IVIM) imaging can provide diffusion and perfusion properties.*
- *However, IVIM or DCE imaging alone is insufficient for diagnosing head/neck tumours.*
- *Multiparametric approach using both IVIM and TIC profiles can facilitate the diagnosis.*

M. Sumi · T. Nakamura (✉)
Department of Radiology and Cancer Biology, Nagasaki University School of Dentistry, 1-7-1 Sakamoto, Nagasaki 852-8588, Japan
e-mail: taku@nagasaki-u.ac.jp

Keywords Diffusion-weighted MR imaging · Intravoxel incoherent motion theory · Contrast-enhanced MR imaging · Head and neck tumours · Differential diagnosis

Abbreviations

IVIM	intravoxel incoherent motion
TIC	time-signal intensity curve
DCE	dynamic contrast-enhanced
PP	perfusion-related parameter
D	molecular diffusion
SCC	squamous cell carcinoma
SPAIR	spectral attenuated with inversion recovery
TSE	turbo spin-echo
MT	maximum time
ER	enhancement ratio
WR	washout ratio
SE	spin-echo
EPI	echo planar imaging

Introduction

Some types of head and neck tumours can occur in the same organs or spaces and should be differentiated in a given clinical context [1]. For example, squamous cell carcinomas (SCCs) and lymphomas, as well as benign and malignant salivary gland tumours occur in the parotid gland. The pharyngeal mucosal space is a platform for many benign and malignant tumours, such as SCCs, lymphomas and salivary gland tumours. In addition, schwannomas may occur in the close vicinity of gland exhibiting conventional magnetic resonance (MR) imaging features similar to those of pleomorphic adenomas [1]. These head and neck tumours may exhibit indistinguishable conventional computed tomography (CT) and magnetic resonance (MR) imaging features. Therefore,

effective differentiation between benign and malignant tumours and between different tumour types is often difficult.

Recently, several attempts have been made to determine the perfusion and diffusion parameters separately by using intravoxel incoherent motion (IVIM) MR imaging [2–5]. The diffusion properties of tumour tissues largely depend on cell density; therefore, they may also be predictive of malignancy in some types of tumours. Perfusion is an important marker of many physiological and pathological processes. For example, the perfusion parameter can be used as a predictive indicator for the effectiveness of chemoradiotherapy [6–8]. Therefore, estimating these two distinctive phenomena in tumour tissues may be helpful in the preoperative diagnosis of tumours. A simplified IVIM MR imaging technique based on the IVIM model has been used to assess perfusion-related parameters (*PP*) and molecular diffusion (*D*) of head and neck tumours and hepatocellular carcinomas [6, 9]. In a study, the *PP* and *D* values were determined graphically with three or four *b* values (0, 500 and 1,000 s/mm^2; or 0, 200, 400 and 800 s/mm^2). This technique is both rapid and easy to apply compared with IVIM imaging using multiple *b* values (e.g. 0, 10, 20, 30, 50, 80, 100, 200, 300, 400 and 800 s/mm^2) [3].

The time-signal intensity curve (TIC) profiles obtained after dynamic contrast-enhanced (DCE) MR imaging represent tumour tissue perfusion properties. However, previous studies have shown significant overlaps in the profiles of apparent diffusion coefficients (ADC) and TIC patterns between benign and malignant salivary gland tumours [10–13]. Therefore, the use of any single technique may not be effective in establishing differentiation criteria for head and neck tumours involving different tumour types with different histologies. In this regard, recent studies have shown that the combined use of diffusion-weighted (DW) and DCE imaging significantly improves diagnostic accuracy in salivary gland tumours [14, 15].

Therefore, in the present study we evaluated whether the combined use of TIC and IVIM parameters provided effective differentiation between benign and malignant head and neck tumours and between different types of head and neck tumours.

Materials and methods

Patients

We retrospectively analysed DW and DCE MR images obtained from 131 patients with head and neck tumours, who received preoperative MR examinations between 2005 and 2010. The other inclusion criteria of this study were:

1. Both DW and DCE MR images were available.
2. Large sizes (>10 mm in short-axis diameters) having enough non-necrotic/cystic areas within the tumours, thereby not significantly limiting the area sufficient for the analyses,
3. Excised tumours were histologically diagnosed.
4. MR images were good in quality without severe susceptibility or motion artefacts.

We excluded ten patients from the study owing to insufficient image quality related to motion artefacts. Consequently, we studied DW and DCE MR images of 92 head and neck tumours from 79 patients with head and neck tumours (37 women and 42 men; average age, 59 years; age range 14–92 years) (Table 1). This retrospective study was approved by the institutional review board. Informed consent was waived off owing to the retrospective nature of this study.

MR imaging

MR imaging was performed using 1.5-T MR (Gyroscan Intera 1.5 T Master; Philips Healthcare, Best, The Netherlands) with a two-channel 11-cm (Synergy-Flex S), 17×14-cm (Synergy-Flex M), 20-cm (Synergy-Flex L) surface coil, or three-channel head and neck coil (Synergy Head Neck; Philips Healthcare, Best, The Netherlands).

T1- and T2-weighted and DCE MR imaging

We obtained axial T1-weighted and fat-suppressed (spectral attenuated with inversion recovery, SPAIR) T2-weighted MR images (TR/TE/number of signal acquisitions=500 ms/15 ms/2 and 6,385 ms/80 ms/2, respectively) by using a turbo spin-echo (TSE) sequence (TSE factor=3 and 15, respectively). We used a 200-mm FOV, 256×204 acquisition and 512×512 reconstruction matrix sizes, a 4-mm slice thickness and a 0.4-mm slice gap. For DCE studies, axial T1-weighted images (TR/TE/number of signal acquisitions=306 ms/10 ms/1) were obtained using a TSE sequence (TSE factor=7), 200×200 mm^2 FOV, 4- to 5-mm slice thickness, 0.4- to 0.5-mm slice gap and 256×180 matrix size. Gadolinium (gadopentetate dimeglumine, Magnevist; Bayer HealthCare, Berlin, Germany) was injected intravenously at a dose of 0.2 ml/kg body weight and at an injection rate of 1.5 ml/s, followed by a 20-ml saline flush. In each patient, 19 MR data acquisitions were obtained at an interval of 10 s (0–180 s). We analysed a single slice of the axial DCE MR image that was obtained from the maximum area of each tumour so that we could analyse a pair of DW and DCE MR images that were obtained from an almost identical part of respective tumours.

TIC analysis

The sequential dynamic MR images in a DICOM format were analysed by using ImageJ and Mathematica (Wolfram Research, Hanborough, UK) software. A freehand ROI (>10 mm) was placed onto a tumour area so that it included as much tumour area as possible on a post-enhanced (180 s) T1-

Table 1 Ninety-two head and neck tumours

Tumours	No. of patients	No. of tumours
SCC[a]	13	18
Lymphoma[b]	25	32
Malignant salivary gland tumours	14	14
adenoid cystic carcinoma	4	
adenocarcinoma	3	
carcinoma ex pleomorphic adenoma	2	
mucoepidermoid carcinoma	2	
acinic cell carcinoma	1	
myoepithelial carcinoma	1	
salivary duct carcinoma	1	
Pleomorphic adenoma	14	14
Warthin tumour[c]	7	8
Schwannoma	6	6
Total	79	92

SCC squamous cell carcinoma

[a] Of 13 patients with SCC, 3 patients had primary and nodal diseases in the neck and 10 patients had nodal disease in the neck alone (two of them each had 2 SCC nodes)

[b] Histological types of lymphoma included 13 diffuse large B cell tumours, 4 adult T-cell leukaemia lymphomas, 3 follicular lymphomas, 3 MALT lymphomas, 1 Burkitt lymphoma, and 1 Hodgkin lymphoma. Of the 25 patients, 14 had extranodal lymphomas and 11 had lymphoma nodes. Four of the 11 patients with lymphoma node had multiple lesions (three patients each had 3 nodal lesions and one had 2 nodal lesions)

[c] One patient with Warthin tumour had two lesions

weighted MR image. Visually identifiable cystic and necrotic areas were excluded from the ROI. Then, the same ROIs were automatically placed onto the other 18 dynamic MR images by repeatedly copying and pasting the initial ROI using ImageJ software (NIH, http://rsweb.nih.gov/ij/index.html). The TIC analysis was performed on a lesion-by-lesion (overall TIC) basis and obtained TICs were categorised into five patterns (Types 1–5) according to the maximum time (MT), enhancement ratio (ER), and washout ratio (WR); as previously described (Fig. 1b) [11]. TIC maps were obtained by automatically analysing DCE data by using the Mathematica software and displayed as two-dimensional distributions of the five TIC patterns (Fig. 2).

DW MR imaging

DW MR imaging was performed before contrast-enhanced MR imaging. Axial DW images (TR/TE/numbers of signal acquisition=4,283 ms/87 ms/4) were obtained using single shot, spin-echo (SE) echo planar imaging (EPI). We used three *b* values (0, 500 and 1,000 s/mm^2). We obtained isotropic diffusion images by applying the two higher *b* factors along the three orthogonal directions using a 200×200 mm^2 FOV, 4-mm slice thickness, 0.4-mm slice gap and 112×90 matrix size. Phase-encoding was applied along the antero-posterior direction. The parallel imaging (sensitivity encoding, SENSE; SENSE factor=2) technique was used for rapid image acquisition and for reducing susceptibility artefact. Imaging time was 2 min and 8 s for the acquisition of 25 slices.

IVIM-based analysis of perfusion-related and molecular diffusion parameters

We analysed a single DW MR image obtained from the maximum area of each tumour. A region of interest (ROI, short-axis diameter >10 mm) was manually placed onto each

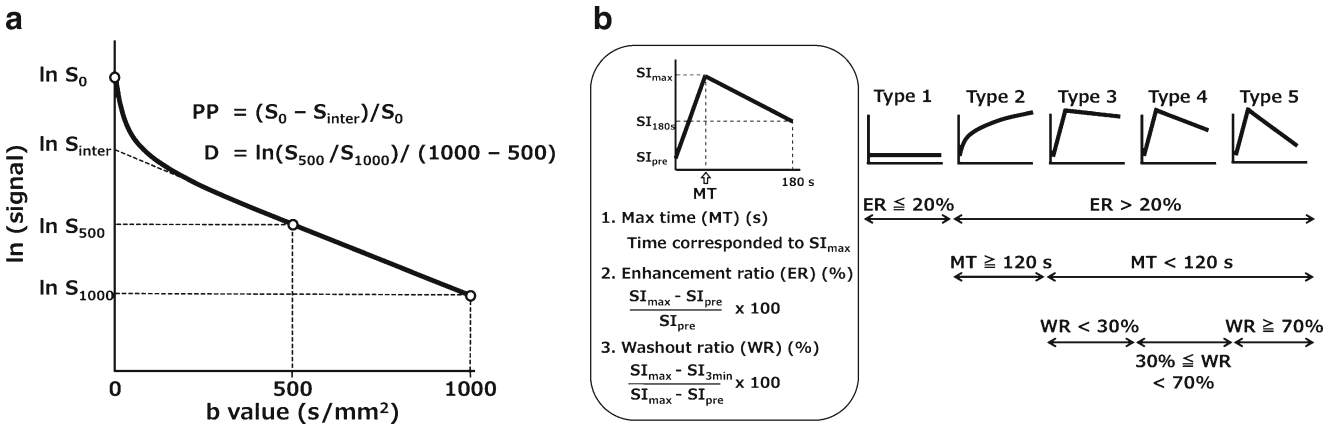

Fig. 1 Intravoxel incoherent motion (IVIM)- and time-signal intensity curve (TIC)-based assessment of tumour perfusion and diffusion. **a** Schema drawn from patient data showing IVIM-based perfusion-related parameter (*PP*) and molecular diffusion (*D*). *PP* is estimated by the equation: $PP=(S_0 - S_{inter})/S_0$, and *D* is calculated by the equation to be: $D=\ln(S_{500}/S_{1,000})/500$. S_0 and S_{inter} signal intensities at $b=0$ s/mm^2 and at interception of the logarithmic regression line obtained using *b* values of 500 and 1,000 s/mm^2 with the *y*-axis, respectively. **b** TIC analysis and classification. The TICs obtained were classified into five types (Types 1–5) based on the enhancement ratio (ER), maximum time (MT), and washout ratio (WR) values (*right panel*). *Type 1* TICs are those with ERs equal to or smaller than 20 %. *Type 2* TICs are those with ERs greater than 20 % and MTs equal to or longer than 120 s, *Type 3* TICs are those having ERs greater than 20 %, with PTs shorter than 120 s and with WRs smaller than 30 %. *Type 4* TICs are those displaying ERs greater than 20 %, with MTs shorter than 120 s and with WRs equal to or greater than 30 % and smaller than 70 %. *Type 5* TICs are those that were not categorised into any of the above types

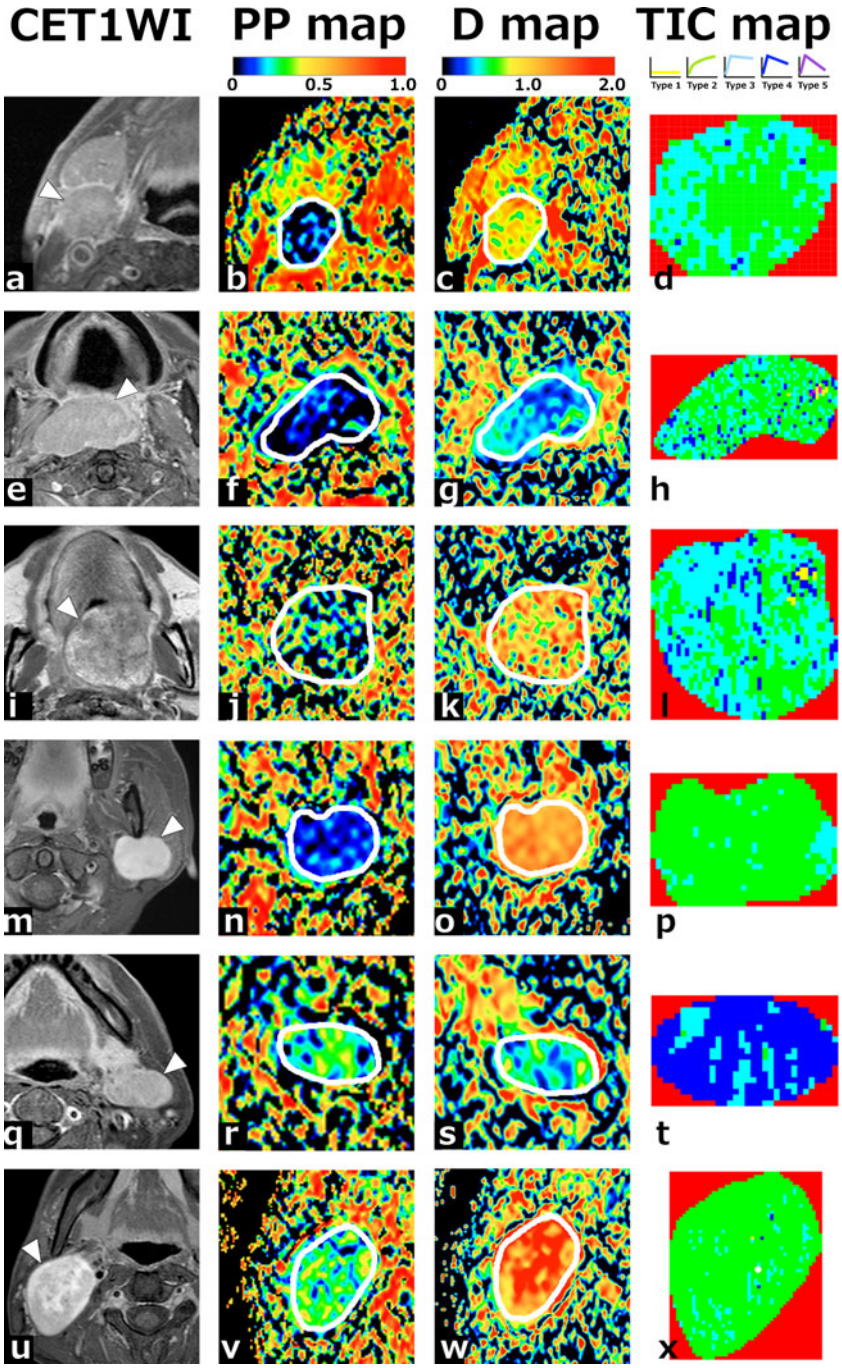

Fig. 2 Representative contrast-enhanced T1-weighted MR images (CET1WI) with (**a**, **e**, **m**, **q** and **u**) or without (**i**) fat-suppression, and *PP*, *D*, and TIC maps of a squamous cell carcinoma (SCC) node (**a**-**d**), lymphoma (**e**-**h**), carcinoma ex pleomorphic adenoma (**i**-**l**), pleomorphic adenoma (**m**-**p**), Warthin tumour (**q**-**t**) and schwannoma (**u**-**x**). **a**-**d** A 75-year-old man with an SCC node at level IIA (**a**). *PP*=0.057 (**b**), $D=0.830\times10^{-3}$ mm^2/s (**c**), TIC profile=Type 2 (**d**). **e**-**h** A 79-year-old man with lymphoma in the oropharynx (**e**), *PP*=0.04 (**f**), $D=0.435\times10^{-3}$ mm^2/s (**g**), TIC profile=Type 3. **i**-**l** A 59-year-old man with carcinoma ex pleomorphic adenoma in the palate (**i**), *PP*=0.217 (**j**), $D=1.005\times10^{-3}$ mm^2/s (**k**), TIC profile=Type 3 (**l**). **m**-**p** A 34-year-old woman with pleomorphic adenoma in the left parotid gland (**m**), *PP*=0.099 (**n**), $D=1.287\times10^{-3}$ mm^2/s (**o**), TIC profile=Type 2 (**p**). **q**-**t** A 63-year-old woman with Warthin tumour in the left parotid gland (**q**), *PP*=0.227 (**r**), $D=0.485\times10^{-3}$ mm^2/s (**s**), TIC profile=Type 4 (**t**). **u**-**x** A 24-year-old man with a schwannoma (**u**), *PP*=0.294 (**v**), $D=1.550\times10^{-3}$ mm^2/s (**w**), TIC profile=Type 2 (**x**).*White demarcations* on the *PP* and *D* maps indicate tumour areas

tumour area of DW MR image such that it encompassed as much of the tumour area as possible. We used DCE MR images as references to determine tumour areas on the corresponding DW images.

The relationship between signal intensities and b values was assessed based on the IVIM theory by using the following equation:

$$S_b/S_0 = (1-f)\cdot exp(-bD) + f\cdot exp[-b(D+D*)] \quad (1)$$

where f is the microvascular volume fraction representing the fraction of the diffusion linked to microcirculation [5]; D is the diffusion parameter representing pure molecular diffusion (diffusion coefficient); D^* is the perfusion-related incoherent microcirculation. S_0 and S_b are signal intensities at $b=0$ s/mm^2 and $b>0$ s/mm^2, respectively (Fig. 1a). By using logarithmic plots, D can be obtained with a linear regression algorithm. Given an estimated D value, the corresponding f and D^* values can be calculated using a non-linear regression algorithm based on the Eq. 1. In the present study, however,

we estimated the tissue perfusion by graphically calculating the perfusion-related parameters (*PP*) as:

$$1–S_{inter}/S_0 \quad (2)$$

where S_{inter} is the interception of the logarithmic regression line obtained using b values of 500 and 1,000 s/mm^2 with the y-axis (Fig. 1) [6, 9]. Accordingly, the *PP* is the variable representing the graphical estimation of f, and is defined as signal decays due to quasi-random proton movement within the capillary network between $b=0$ and $b=500$ s/mm^2.

DW images in a DICOM format were converted to 2D colour maps of *PP* and *D* values using ImageJ software (Fig. 2).

Interobserver errors

All the DWI and TIC analyses were performed by a radiologist with 17 years' experience in the field of head and neck diagnostic radiology. Separate MR images from ten head and neck tumours were analysed independently by two radiologists with 17 years' experience to assess interobserver errors by calculating coefficient of variation (CV).

Statistics

Shapiro-Wilk and Tukey-Kramer HSD tests were used for the comparison of the IVIM parameters among the four different types of head and neck tumours. Cluster analysis was used to determine the best threshold for the IVIM criteria for discriminating between different tumour groups, where the best cut-off IVIM values were determined so that the values differentiated with the highest accuracy between different tumour groups that were categorised by Ward's method using a dendrogram. The statistical analyses were performed using SPSS (version 18.0; IBM Corporation, Armonk, NY, USA) and Excel Statistics 2012 (version 1.00; SSRI, Tokyo, Japan).

Results

Conventional MR imaging

Conventional T1-weighted and fat-suppressed T2-weighted MR images of 92 head and neck tumours exhibited considerably overlapping signal intensity profiles of benign and malignant tumours and of different tumour types (Table 2). Therefore, differentiation of different tumour types was difficult based on conventional MR imaging.

Interobserver errors

Interobserver errors were 1.19 % CV and 3.98 % CV for *D* and *PP* values, respectively. TIC categorisation was completely matched between the two observers.

IVIM-based differentiation of head and neck tumours

The head and neck tumours analysed had a broad range of *PP* and *D* values (Table 3, Figs. 2, 3 and 4). Tukey-Kramer analyses revealed that the *PP* values of lymphomas and pleomorphic adenomas were significantly ($P<0.01$) smaller than those of malignant salivary gland tumours, Warthin tumours and schwannomas (Fig. 3). The *PP* values of SCCs were significantly different from those of lymphomas ($P<0.01$), malignant salivary gland tumours ($P<0.05$), Warthin tumours ($P<0.05$) and schwannomas ($P<0.01$), but not from those of pleomorphic adenomas. However, considerable overlaps were present between many types of head and neck tumour.

Tukey-Kramer analysis revealed that the *D* values were significantly ($P<0.05$ or 0.01) different among some types of tumours, but the values also overlapped considerably (Fig. 4). These results suggest that single use of the IVIM parameter or TIC profile is insufficient for differentiating different types of head and neck tumours.

TIC analysis of head and neck tumours

TIC profiles did not correlate with the *PP* values (Table 3). For instance, schawannomas, Warthin tumours and malignant salivary gland tumours had similarly high *PP* values, but the TIC profiles differed greatly among the tumour types.

A stepwise approach for differentiating head and neck tumours

Given that the single use of either IVIM parameters or TIC profiles was not effective for differentiating tumours, we next attempted to discriminate tumours with the combined use of IVIM parameters (*PP* and *D*) and TIC profiles. Accordingly, we conducted a stepwise approach with TIC-based categorisation performed as the first step (Fig. 5). Type 2 TIC profiles (slow uptake) were characteristic of many types of head and neck tumours (Table 3; Fig. 5, *left panel*). However, the *D* values of lymphomas (D <0.6×10^{-3} mm^2/s), SCCs (0.6-1.0×10^{-3} mm^2/s) and malignant salivary gland tumours (1.0-1.2×10^{-3} mm^2/s) were distinctive and *PP* values were distinctive between pleomorphic adenomas (*PP* <1.7) and schwannomas (*PP* ≥1.7), which both had high *D* values (≥1.2×10^{-3} mm^2/s).

Tumours with Type 3 TIC profiles (rapid uptake with low WR) were categorised into those with small *D* values (<0.6×10^{-3} mm^2/s, lymphomas) and those with large *D* values

Table 2 Conventional MR images of 92 head and neck tumours

	T1WI (%)				fsT2WI (%)				Total
	homo		hetero		homo		hetero		
Benign									
Pleomorphic adenoma	11	(79)	3	(21)	2	(14)	12	(86)	14
Schwannoma	4	(67)	2	(33)	1	(17)	5	(83)	6
Warthin tumour	3	(38)	5	(63)	3	(38)	5	(63)	8
Malignant									
Malignant salivary gland tumour	7	(50)	7	(50)	0	(0)	14	(100)	14
Lymphoma	32	(100)	0	(0)	31	(97)	1	(3)	32
SCC	18	(100)	0	(0)	6	(33)	12	(67)	18

T1-weighted (*T1WI*) and fat-suppressed T2-weighted (*fsT2WI*) MR images of 92 head and neck tumours were visually evaluated for their homogeneity (*homo* homogeneous or *hetero* heterogeneous) by a radiologist with 17 years' experience

($\geq 0.6\times10^{-3}$ mm^2/s, SCCs and malignant salivary gland tumours; Fig. 5, *centre panel*). Malignant salivary gland tumours were further discriminated from SCCs based on a *PP* criterion (*PP* ≥0.17).

Among the tumours with Type 4 TIC profiles (rapid uptake with high WR), Warthin tumours had larger *PP* values (≥0.17), while lymphomas and lymphoma nodes had smaller *PP* values (<0.17; Fig. 5, *right panel*).

Consequently, the stepwise approach with the combined use of TIC profiles and IVIM parameters differentiated between benign and malignant tumours with 97 % (89/92) accuracy, while the same MR criteria diagnosed 89 % (82/92) of the different tumour types correctly. Therefore, we characterised the head and neck tumours according to the TIC profile and IVIM parameters (Table 4), showing that the combined use of IVIM and TIC parameters can effectively differentiate different types of head and neck tumours.

Discussion

Intravoxel incoherent motion MR imaging is a technique with the potential for simultaneously assessing both tissue perfusion and diffusion by using a single DW imaging. On the other hand, perfusion clearly relates to DCE MR imaging. In the present study, we have shown that the combined use of perfusion (*PP* values, which are analogous to *f*, and TIC patterns) and diffusion (*D* values) parameters as assessed by DW and DCE MR imaging effectively differentiated between benign and malignant head and neck tumours and also discriminated between head and neck tumours with different histological types with high accuracy.

The TIC analysis with DCE MR imaging can estimate the physiological properties of different tissue components based on their blood flow [10]. Differentiation between benign and malignant salivary gland tumours is an example of the successful application of this technology [12]. However, effective discrimination between head and neck tumours with different histological types has proved difficult. For example, some lymphomas that occurred in the parotid glands had TIC profiles similar to Warthin tumours and other lymphomas exhibited Type 2 TIC patterns that were often observed in SCCs and pleomorphic adenomas [10, 16].

The basic concept of IVIM imaging established by Le Bihan requires multiple *b* values [3–5, 17]. However, the use of multiple *b* values requires extended image acquisition time and additional post-processing time. Furthermore, the complicated method for estimating fit f and D* values by

Table 3 IVIM and TIC characteristics of 92 head and neck tumours

Tumours	*n*	IVIM parameters		Overall TIC patterns (%)		
		PP	*D* ($\times 10^{-3}$ mm^2/s)	Type 2	Type 3	Type 4
Benign						
Pleomorphic adenoma	14	0.11±0.03	1.59±0.39	13 (93)	1 (7)	0 (0)
Schwannoma	6	0.22±0.05	1.40±0.14	6 (100)	0 (0)	0 (0)
Warthin tumour	8	0.20±0.04	0.62±0.13	0 (0)	0 (0)	8 (100)
Malignant						
Malignant SG tumour	14	0.19±0.06	0.96±0.23	6 (43)	8 (57)	0 (0)
Lymphoma	32	0.08±0.04	0.46±0.08	4 (13)	12 (38)	16 (50)
SCC	18	0.14±0.04	0.73±0.11	6 (33)	11 (61)	1 (6)

IVIM intravoxel incoherent motion, *TIC* time-signal intensity curve, *PP* perfusion-related parameter, *D* molecular diffusion, *WR* washout ratio, *SG* salivary gland, *SCC* squamous cell carcinoma

Please see Fig. 1b for the definitions of TIC profiles (Types 2, 3 and 4)

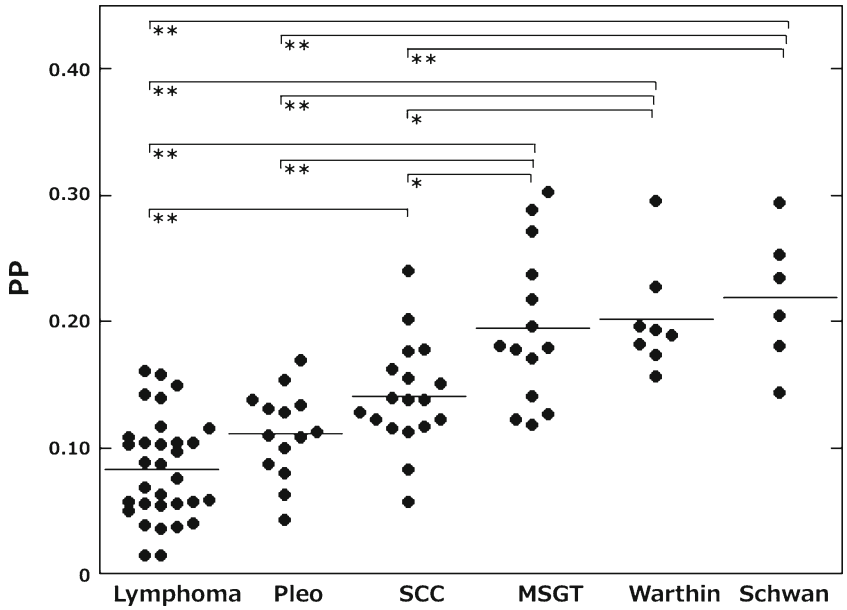

Fig. 3 The *PP* values of different types of head and neck tumour. Significantly different *PP* values at $P<0.05$ (*) or $P<0.01$ (**), Tukey-Kramer HSD test. *Pleo* pleomorphic adenoma, *SCC* squamous cell carcinoma, *MSGT* malignant salivary gland tumour, *Warthin* Warthin tumour, *Schwan* schwannoma

using a non-linear regression algorithm may increase errors and make data interpretation problematic. The simplified graphical estimation of IVIM parameters may be beneficial for routine clinical situations. However, the simplified technique might be achieved at the expense of accuracy in estimating the tumour perfusion [9]. To evaluate the utility of the graphical estimation of IVIM parameters, we compared IVIM values that were estimated by the least squares method using 11 *b* values and the graphical estimation from a separate patient cohort. We found that the two estimation methods yielded similar diagnostic accuracy in differentiating between benign and malignant tumours and between different types of head and neck tumours such as SCCs, lymphomas, pleomorphic adenomas, Warthin tumours and malignant salivary gland tumours (data not shown). Therefore, we propose the graphical estimation of *f* and *D* values as an alternative method of assessing tissue perfusion [6, 9].

In the present study, the combined use of TIC and IVIM criteria improved the diagnostic ability compared with the use of IVIM or TIC criteria alone. For instance, a *PP* criterion effectively discriminated lymphomas and lymphoma nodes with Type 4 TIC profiles from Warthin tumours with the same TIC profile. The same *PP* criterion effectively differentiated between pleomorphic adenomas and schwannomas with Type

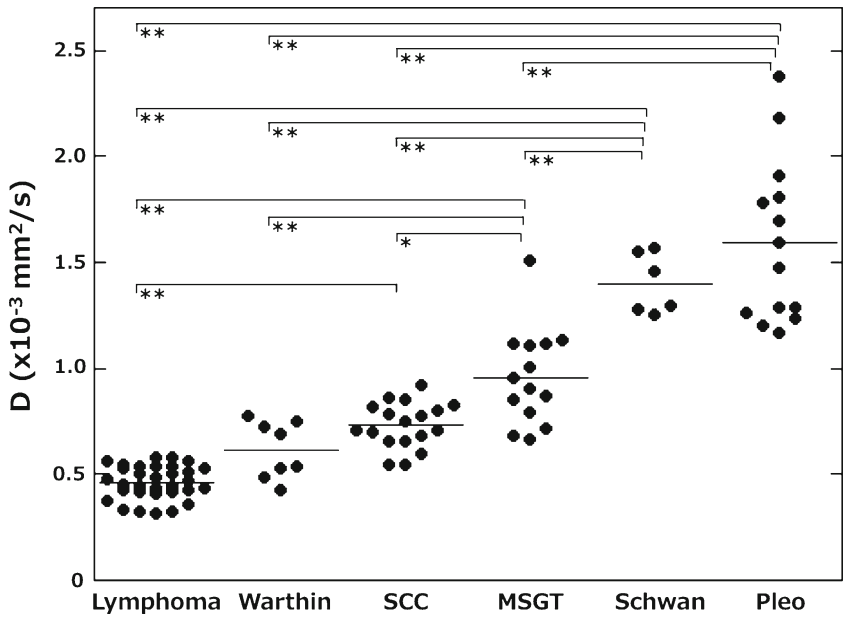

Fig. 4 D values of different types of head and neck tumour. Significantly different *PP* values at $P<0.05$ (*) or $P<0.01$ (**), Tukey-Kramer HSD test. *Pleo* pleomorphic adenoma, *SCC* squamous cell carcinoma, *MSGT* malignant salivary gland tumour, *Warthin* Warthin tumour, *Schwan* schwannoma

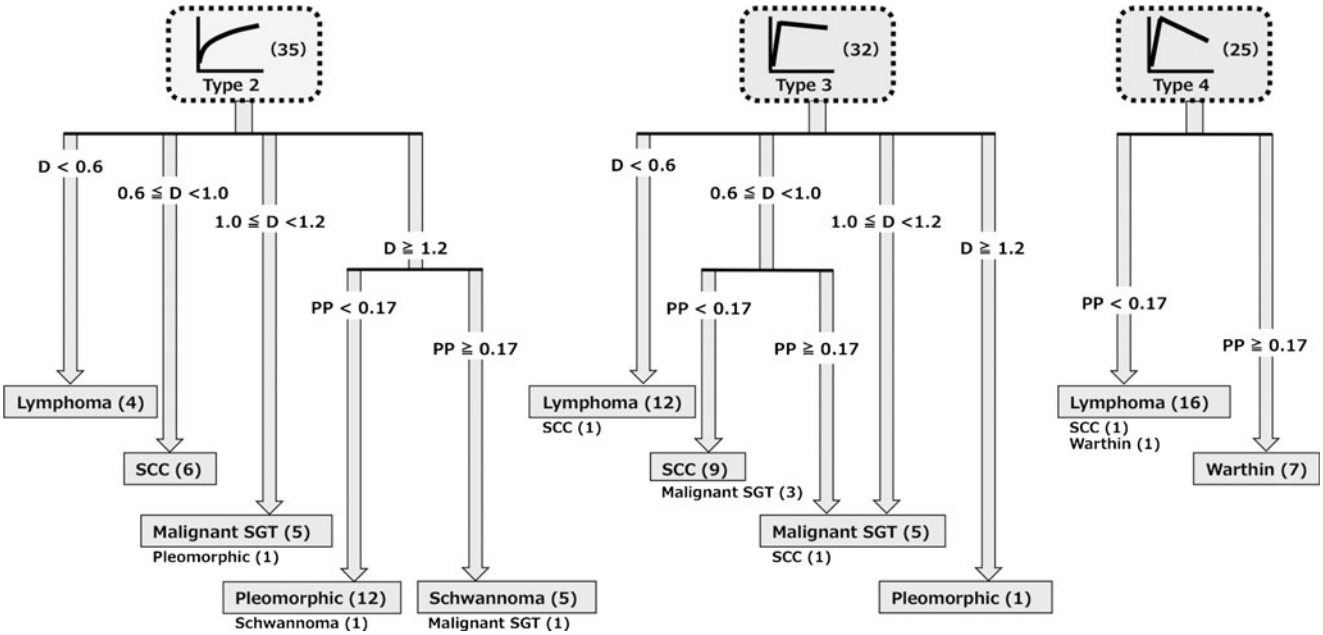

Fig. 5 Stepwise differentiation of different types of head and neck tumours using DCE (TIC profile) and DW (*D* and *PP* values) parameters. At the first step, TIC analysis categorised 92 tumours into those with Type 2 TIC profiles, Type 3 TIC profiles or Type 4 TIC profiles. Then, the tumours in each category were further classified into particular tumour types according to the *D* and *PP* levels based on the cluster analysis. Consequently, 89 (97 %) of the 92 tumours were correctly diagnosed as benign or malignant; and 82 (89 %) of the 92 tumours were correctly diagnosed as a specific type of head and neck tumour. The incorrect results (*outside the frames*) included: one pleomorphic adenoma with Type 2 TIC profile and an intermediate *D* value (1.17×10^{-3} mm^2/s); one myoepithelial carcinoma with Type 2 TIC profile, a large *D* value (1.51×10^{-3} mm^2/s) and a large *PP* value (0.30); one schwannoma with Type 2 TIC profile and a small *PP* value (0.14); one SCC node with Type 3 TIC profile and a small *D* value (0.55×10^{-3} mm^2/s); two adenocarcinomas with Type 3 TIC profile and small *PP* values (0.12 and 0.14); one salivary duct carcinoma with Type 3 TIC profile and a small *PP* value (0.13); one SCC with Type 3 TIC profile and a large *PP* value (0.20); one SCC node with Type 4 TIC profile and a small *PP* value (0.16); one Warthin tumour with Type 4 TIC profile and a small *PP* value (0.16). $D = \times 10^{-3}$ mm^2/s. *D* molecular diffusion, *PP* perfusion-related parameter, *SCC* squamous cell carcinoma, *SGT* salivary gland tumour, pleomorphic, pleomorphic adenoma, *Warthin* Warthin tumour. The *numbers in the parentheses* to the TIC profiles and tumour types indicate the numbers of tumours

2 TIC profiles and high *D* values. These results suggest that TIC parameters and *PP* values reflect different aspects of tumour perfusion properties.

Table 4 TIC and IVIM criteria of head and neck tumours

Tumours	TIC profile	*D* ($\times10^{-3}$ mm^2)	*PP*
Schwannoma	Type 2	≥1.2	≥0.17
Pleomorphic adenoma	Type 2	≥1.2	<0.17
Malignant SG tumour	Type 2	1.0-1.2	-
	Type 3	0.6-1.2	≥0.17
SCC	Type 2	0.6-1.0	-
	Type 3	0.6-1.0	<0.17
Lymphoma	Type 2	<0.6	-
	Type 3	<0.6	-
	Type 4	-	<0.17
Warthin tumour	Type 4	-	≥0.17

TIC time-signal intensity curve, *D* molecular diffusion, *PP* perfusion-related parameter, *SG* salivary gland, *SCC* squamous cell carcinoma; - variable

Considering the broad spectrums and considerable overlaps in the diffusion and perfusion properties of head and neck tumours, we have attempted to achieve high accuracy in differentiating between benign and malignant tumours by using a stepwise approach. The first step was performed using TIC analysis with DCE MR imaging. The second step was performed using IVIM parameters with DW MR imaging. Consequently, we differentiated between benign and malignant head and neck tumours with high accuracy. We also effectively discriminated between different tumour types; however, ten (11 %) of the 92 tumours were incorrectly diagnosed with the stepwise differentiation system because the *D* or *PP* values did not fulfil the criteria for each tumour type. Therefore, the *D* and *PP* criteria proposed in the present study are provisional and need some modifications in the future.

A previous study showed that a combination of *D* and *D** criteria provided 100 % accuracy in differentiation among different types of salivary gland tumours [3]. Nevertheless, the performance of this set of IVIM parameters (*D* and *D**) was found to be limited for a broader spectrum of head and neck tumours [9]. However, in the present study the combined

use of perfusion (graphically determined *PP*, which is analogous to *f*, and the TIC profiles) and diffusion (*D*) criteria provided insufficient diagnostic accuracy in differentiating between different types of salivary gland tumours. Therefore, in a given clinical context (in this case, differentiation of salivary gland tumours), TIC analysis may not be needed for effective diagnosis.

A major limitation of this study is that the study cohort was small. A similar analysis on a larger cohort containing greater numbers and types of head and neck tumours might provide different *D* and *PP* criteria for improved results [3, 9]. Another major limitation of this study is the constraint on tumour size in the TIC and IMVIM analyses. As stated in the methods section, we excluded tumours that did not have a large enough size for analysis. This problem may be a serious restriction, especially in diagnosing SCC and lymphoma nodes in the neck [18, 19]. The use of a small surface coil or a 3.0-T MR system, or both could potentially alleviate this problem. Additional drawbacks of this study included that: (1) we assessed primary and metastatic SCC nodes together; however, tumour biology in the primary might differ from the corresponding lymph node; (2) in lymphomas and most benign lesions, a single slice of a tumour is sufficient for the analysis; however, in SCCs there will be considerable heterogeneity due to fast growth and insufficient blood supply leading to necrosis.

In conclusion, a multiparametric approach using time-signal intensity curve and intravoxel incoherent motion criteria differentiated between benign and malignant head and neck tumours and between head and neck tumours of different histological types with high accuracy.

Acknowledgements Some patients of the present study cohort overlapped those of the previous study, which was published in the *American Journal of Neuroradiology* [9]. In that paper, we evaluated IVIM parameters for diagnosing head and neck tumours, but not the combined assessment of TIC and IVIM parameters.

References

1. Harnsberger HR, Wiggins RH, Hudgins PA et al (2004) Diagnostic Imaging Head and Neck. AMIRSYS, Salt Lake City
2. Le Bihan D (2003) Looking into the functional architecture of the brain with diffusion MRI. Nat Rev Neurosci 4:469–480
3. Sumi M, Van Cauteren M, Sumi T, Obara M, Ichikawa Y, Nakamura T (2012) Salivary gland tumors: use of intravoxel incoherent motion MR imaging for assessment of diffusion and perfusion for the differentiation of benign from malignant tumors. Radiology 263:770–777
4. Luciani A, Vignaud J, Cavet M et al (2008) Liver cirrhosis: intravoxel incoherent motion MR imaging—pilot study. Radiology 249:891–899
5. Guiu B, Petit JM, Capitan V et al (2012) Intravoxel incoherent motion diffusion-weighted imaging in nonalcoholic fatty liver disease: a 3.0-T MR study. Radiology 265:96–103
6. Lewin M, Fartoux L, Vignaud A, Arrivé L, Menu Y, Rosmorduc O (2011) The diffusion-weighted imaging perfusion fraction f is a potential marker of sorafenib treatment in advanced hepatocellular carcinoma: a pilot study. Eur Radiol 21:281–290
7. Kim S, Loevner LA, Quon H et al (2010) Prediction of response to chemoradiation therapy in squamous cell carcinomas of the head and neck using dynamic contrast-enhanced MR imaging. AJNR Am J Neuroradiol 31:262–268
8. Chawla S, Kim S, Loevner LA et al (2011) Prediction of disease-free survival in patients with squamous cell carcinomas of the head and neck using dynamic contrast-enhanced MR imaging. AJNR Am J Neuroradiol 32:778–784
9. Sumi M, Nakamura T (2013) Head and neck tumors: assessment of perfusion-related parameters and diffusion coefficients based on the intravoxel incoherent motion model. AJNR Am J Neuroradiol 34:410–416
10. Eida S, Ohki M, Sumi M, Yamada T, Nakamura T (2008) MR factor analysis: improved technology for the assessment of 2D dynamic structures of benign and malignant salivary gland tumors. J Magn Reson Imaging 27:1256–1262
11. Sasaki M, Sumi M, Eida S et al (2011) Multiparametric MR imaging of sinonasal diseases: time-signal intensity curve- and apparent diffusion coefficient-based differentiation between benign and malignant lesions. AJNR Am J Neuroradiol 32:2154–2159
12. Yabuuchi H, Fukuya T, Tajima T, Hachitanda Y, Tomita K, Koga M (2002) Salivary gland tumors: diagnostic value of gadolinium-enhanced dynamic MR imaging with histopathologic correlation. Radiology 226:345–354
13. Eida S, Sumi M, Sakihama N, Takahashi H, Nakamura T (2007) Apparent diffusion coefficient mapping of salivary gland tumors: prediction of the benignancy and malignancy. AJNR Am J Neuroradiol 28:116–121
14. Yabuuchi H, Matsuo Y, Kamitani T et al (2008) Parotid gland tumors: can addition of diffusion-weighted MR imaging to dynamic contrast-enhanced MR imaging improve diagnostic accuracy in characterization? Radiology 249:909–916
15. Eida S, Sumi M, Nakamura T (2010) Multiparametric magnetic resonance imaging for the differentiation between benign and malignant salivary gland tumors. J Magn Reson Imaging 31:673–679
16. Furukawa M, Parvathaneni U, Maravilla K, Richards TL, Anzai Y (2013) Dynamic contrast-enhanced MR perfusion imaging of head and neck tumors at 3 Tesla. Head Neck 35:923–929
17. Sigmund EE, Cho GY, Kim S (2011) Intravoxel incoherent motion imaging of tumor microenvironment in locally advanced breast cancer. Magn Reson Med 65:1437–1447
18. Nakamura T, Sumi M (2007) Nodal imaging in the neck: recent advances in US, CT, and MR imaging of metastatic nodes. Eur Radiol 17:1235–1241
19. Sumi M, Nakamura T (2009) Diagnostic importance of focal defects in the apparent diffusion coefficient-based differentiation between lymphoma and squamous cell carcinoma nodes in the neck. Eur Radiol 19:975–981